Journal of Solid State Chemistry 182 (2009) 2858–2866

Contents lists available at ScienceDirect

Journal of Solid State Chemistry

journal homepage: www.elsevier.com/locate/jssc

Structural characterisation of the perovskite series $Sr_xCa_{1-x-y}Nd_yMnO_3$: Influence of the Jahn–Teller effect

Brendan J. Kennedy [a,*], Paul J. Saines [a], Jimmy Ting [a], Qingdi Zhou [a], Justin A. Kimpton [b]

[a] School of Chemistry, The University of Sydney, New South Wales 2006, Australia
[b] Australian Synchrotron, 800 Blackburn Road, Clayton, Victoria 3168, Australia

ARTICLE INFO

Article history:
Received 22 April 2009
Received in revised form
13 July 2009
Accepted 18 July 2009
Available online 6 August 2009

Keywords:
Perovskite
Structural phase transition
Isosymmetric phase transition
Manganites

ABSTRACT

The crystal structures of the perovskite manganites $Sr_xCa_{1-x-y}Nd_yMnO_3$ with $y = 0.1$ or 0.2 have been investigated using synchrotron X-ray powder diffraction. At room temperature the structures change from $Pm\bar{3}m \leftrightarrow I4/mcm \leftrightarrow Pbnm$ depending on the cation distribution, the different structures exhibiting different tilts of the MnO_6 octahedra. High temperature diffraction measurements demonstrate the presence of, an apparently continuous, isosymmetric $I4/mcm$ to $I4/mcm$ phase transition associated with the removal of long range orbital ordering. Heating the manganites to still higher temperatures results in a continuous transition to the cubic $Pm\bar{3}m$ structure. A feature of such transitions is the continuous evolution of the octahedral tilt angle through the $I4/mcm$ to $I4/mcm$ phase transition. The orthorhombic structures do not exhibit orbital ordering and although a first order transition to the tetragonal structure is observed in $Sr_{0.4}Ca_{0.5}Nd_{0.1}MnO_3$, this high temperature tetragonal structure does not exhibit orbital ordering.

1. Introduction

In 1937 Jahn and Teller proposed that non-linear degenerate molecules cannot be stable and that any highly symmetrical molecule will undergo a geometric distortion to reduce its symmetry and thereby lower its energy [1]. Since then the Jahn–Teller (JT) effect has continuously attracted interest of chemists and physicists, initially to gain a fundamental understanding of the properties of molecules and crystals, but increasingly to explain technologically important, but complex, phenomena such as superconductivity in the cuprates [2] and magnetoresistance in the manganites [3,4]. The complex interplay between the structure and the magnetic and electronic properties in perovskite manganites has motivated numerous studies over the past few decades, especially of mixed valent oxides of the general type $A_{1-x}R_xMnO_3$ where A is an alkaline earth cation and R a lanthanide cation [3]. There are numerous examples of unusual properties of such oxides that are strongly influenced by the distortions associated with the presence of the JT active Mn^{3+} (d^{4+}) cation [3,5]. For example it is widely accepted that the phase competition between a ferromagnetic metal and charge or orbital ordered insulator is essential for the colossal magnetoresistance (CMR) effect. Orbital ordering (*OO*) is a feature of a cooperative Jahn–Teller distortion (CJTD) [3].

In recent papers we have presented structural studies of some Ce containing strontium manganites [6–8]. It was observed that doping the cubic polytype of $SrMnO_3$ with Ce, to form $Sr_{1-x}Ce_xMnO_3$, induces two abrupt phase transitions, initially to a tetragonal structure in $I4/mcm$ near $x = 0.075$ that involves both long range ordering of the JT elongated MnO_6 octahedra and cooperative tilting of the MnO_6 octahedra, and at still higher Ce contents $x = 0.3$, to an orthorhombic structure in *Imma* [6,9]. Heating tetragonal $Sr_{0.9}Ce_{0.1}MnO_3$ to above 210 °C results in a continuous transition to the archetypal cubic ($Pm\bar{3}m$) perovskite structure. It is possible to partially replace Sr with Ca to form the oxides $Sr_{0.9-x}Ca_xCe_{0.1}MnO_3$ [8]. At room temperature the Ca rich members of this series have an orthorhombic structure in *Pbnm* that is characterised by relatively regular MnO_6 octahedra indicating the absence of a static JT effect. Whilst not fully understood, it is widely observed that orbital ordering rarely occurs in orthorhombic *Pbnm* manganese perovskites, an obvious and important exception being $LaMnO_3$ [10]. The Sr rich samples in the $Sr_{0.9-x}Ca_xCe_{0.1}MnO_3$ series, however, have a tetragonal structure in $I4/mcm$ with the MnO_6 octahedra exhibiting a noticeable elongation due to orbital ordering [8]. Heating selected members of this series results in a transition to the cubic perovskite structure where both the octahedral tilting and elongation are lost. Intriguingly the transformation to cubic symmetry apparently involves two distinct transitions; the first is due to the removal of the orbital ordering and the second the loss of the octahedral tilting. The temperature at which the first of these transitions occurs appears to be insensitive to the Ca:Sr

* Corresponding author.
E-mail address: B.Kennedy@chem.usyd.edu.au (B.J. Kennedy).

0022-4596/$ - see front matter © 2009 Elsevier Inc. All rights reserved.
doi:10.1016/j.jssc.2009.07.041

ratio, whereas the transition temperature for the second of these increases noticeably with increasing Ca (and decreasing Sr) content [8].

Apparently sequential transitions were also observed upon heating the mixed *B*-site perovskite $SrRu_{0.5}Mn_{0.5}O_3$ that also adopts a tetragonal *I*4/*mcm* structure at room temperature [11]. This oxide exhibits a complex redox distribution between Ru^{4+}–Mn^{4+} and Ru^{5+}–Mn^{3+}, and as in the $Sr_{1-x}Ce_xMnO_3$ oxides it is difficult to quantify the amount of JT-active Mn^{3+} present. In the pure Mn^{3+} oxide Sr_2MnSbO_6 a tetragonal to cubic transition is observed, and in this case the evidence suggests simultaneous loss of both the CJTD and the octahedral tilting [12]. Knizek et al. described the structures of the $Sr_{1-x}Pr_xMnO_3$ series with $x \geq 0.55$ [13]. The sequence of structures exhibited by these oxides is the same as found in the $Sr_{1-x}Ce_xMnO_3$ series, namely $Pm\bar{3}m \leftrightarrow I4/mcm \leftrightarrow Imma$ [6,9]. Kolesnik et al. [14] demonstrated correlation between the magnetic and crystal structures and reported a first order transition in $Sr_{0.86}Pr_{0.14}MnO_3$ near 240 K. These workers also reported the presence of sequential magnetic transitions. This work was later extended to include $Sr_xLa_{1-x}MnO_3$ [15] a feature of this series being the presence of a rhombohedral $R\bar{3}c$ phase at higher La contents. Knizek et al. [13] reported that heating samples with low Pr contents $x \leq 0.40$ results in an apparently continuous transition from *I*4/*mcm* to $Pm\bar{3}m$ [13]. The published results do not provide evidence that this occurs in two steps; however, we note that Knizek et al. [13] focused predominantly on the magnetic properties of these samples and only utilised a conventional X-ray powder diffractometer in their high temperature studies, that revealed the presence of the rhombohedral phase observed in the $Sr_xLa_{1-x}MnO_3$ oxides. Evidently there is some considerable variability in these structures.

The above studies suggest sequential continuous phase transitions can occur in some JT distorted manganites. The observation of an apparently continuous isosymmetric phase transition is in conflict with the conclusions of Christy who showed such transitions should be first order [16]. An added complication for the Ce containing oxides is the observation that the Ce exists as a mixture of Ce^{3+} and Ce^{4+} in some of the targeted compositions [7]. This limits the ability of previous studies to establish the amount of the JT active Mn^{3+} cation present. In order to eliminate the potential impact of the valency of other cations on the phase transition we have prepared and structurally characterised two series of oxides $Sr_xCa_{0.9-x-y}Nd_yMnO_3$ ($y = 0.1$ or 0.2) in the knowledge that the Nd will be present as Nd^{3+}. The aim of this paper is to describe results of synchrotron X-ray powder diffraction studies of the structures and phase transition in these two series. Such heavily doped manganites have not been widely studied.

2. Experimental

All reagents were obtained from Aldrich Chemicals with the alkaline earth carbonates and Nd_2O_3 being dried overnight at 100 and 1000 °C, respectively, before use. Samples in the two series $Sr_xCa_{0.9-x-y}Nd_yMnO_3$ ($x = 0$, 0.1, 0.2,… and $y = 0.1$ or 0.2) were synthesised by grinding stoichiometric quantities of $CaCO_3$, $SrCO_3$, Nd_2O_3 and MnO_2 using an agate mortar and pestle and then heating these at 800 °C for 12 h. The samples were next heated, as pellets, to a maximum temperature of 1450 °C for several days, until they appeared as a single phase using a conventional X-ray diffractometer. Such X-ray diffraction patterns were collected using Cu*K*α radiation on a Shimadzu S-6000 diffractometer.

High-resolution synchrotron X-ray powder diffraction studies were performed using MYTHEN microstrip detector on the powder diffractometer at BL-10 of the Australian Synchrotron, Melbourne, Australia [17]. The finely ground powders were placed in 0.3 mm glass or quartz capillaries, as appropriate, that were rotated during the measurements. Data were collected with a 2θ-range between 5° and 85° using the wavelength $\lambda = 0.8270$ Å selected with a Si (111) double crystal monochromator. The uncertainty of the wavelength, estimated from analysis of a diffraction pattern of LaB_6, is $< \pm 0.0001$ Å. Variable temperature data were collected using a Cyberstar hot air blower. The temperature stability was estimated to be better than ±1° above 150 °C and around ±2° below this. Rietveld refinements from the powder diffraction data were carried out with the program Rietica [18] using the atomic scattering factors provided by the program. A pseudo-Voigt function was chosen to generate the line shape of the diffraction peaks. The background was estimated by linear interpolation between around 40 selected points. No regions were excluded in the refinements.

3. Results and discussion

The appropriate space group for the $Sr_xCa_{0.9-x-y}Nd_yMnO_3$ ($y = 0.1$ or 0.2) manganite perovskites was established through examination of both the nature of the superlattice reflections associated with the tilting of the octahedra and the observed pattern of splitting of the Bragg reflections from the parent primitive cell. Fig. 1 illustrates portions of the diffraction patterns for members in the series $Sr_xCa_{0.9-x}Nd_{0.1}MnO_3$ studied in the present work. The diffraction patterns of the Sr rich compounds, $x = 0.8$ and 0.9, did not show any evidence for splitting of the main Bragg reflections, such as the (222) near 2θ~44° ($d = 1.103$ Å; $\lambda = 0.8270$ Å), nor was evidence for any *R*- or *M*-point reflections associated, with out-of-phase or in-phase tilting of the MnO_6 octahedra found. The appropriate space group is cubic $Pm\bar{3}m$ in which undistorted corner-sharing MnO_6

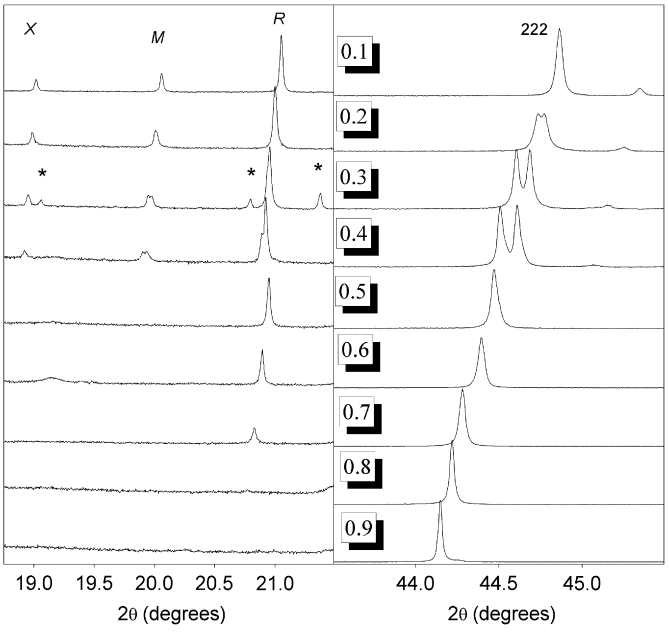

Fig. 1. Selected portions of the observed synchrotron X-ray powder diffraction patterns for members in the series $Sr_xCa_{0.9-x}Nd_{0.1}MnO_3$. The *R*-point reflection near 2θ~21° is indicative of out-of-phase tilting, while the *M*-point reflection near 2θ~20° is indicative of in-phase tilting, of the MnO_6 octahedra. Together with the splitting of the (222) reflection these demonstrate the Ca rich samples to be orthorhombic. The intensities of the plots have been scaled to highlight the appropriate features. The weak peaks marked * are due to a small amount hexagonal $P6_3/mmc$ phase present in the $x = 0.3$ sample.

octahedra are stacked three dimensionally and the *A*-type cations occupy 12-coordinate sites between the octahedra. In the diffraction pattern for $Sr_{0.7}Ca_{0.2}Nd_{0.1}MnO_3$ ($x = 0.7$), a number of *R*-point reflections such as the (121) peak near $2\theta \sim 21^\circ$ are clearly evident and although the (222) reflection remains a singlet the cubic (211) reflection (not illustrated) is split into two well separated reflections indexed as (204) and (312) for a $\sqrt{2}a_p \times \sqrt{2}a_p \times 2a_p$ superstructure, where the subscript p denotes the pseudo-cubic subcell. Thus the structure is tetragonal with $c/a > 1$ and has only out-of-phase tilting of the MnO_6 octahedra about the *c*-axis demonstrating *I*4/*mcm* to be the appropriate space group [19]. In Glazer's [20] notation the structure has the $a^0a^0c^-$ tilt system. The rotation and elongation of the MnO_6 octahedra around and along the *c*-axis, respectively, results in two equivalent apical oxygen atoms, O(1) and four equivalent in-plane oxygen atoms, O(2). As the Ca content is increased further to $x = 0.4$ the (222) reflection is observed to split and apparently simultaneously a number of *M*-point reflections such as the (210) near $2\theta \sim 20^\circ$ appear. The presence of both in- and out-of-phase tilting of the octahedra together with the splitting of the (222) reflection demonstrate the structure is orthorhombic in *Pbnm*, with the corresponding Glazer notation being $a^-a^-c^+$. Intriguingly at still higher Ca contents $x < 0.2$, the splitting of the 222 reflection became increasingly small, although weak *R*-, *M*- and

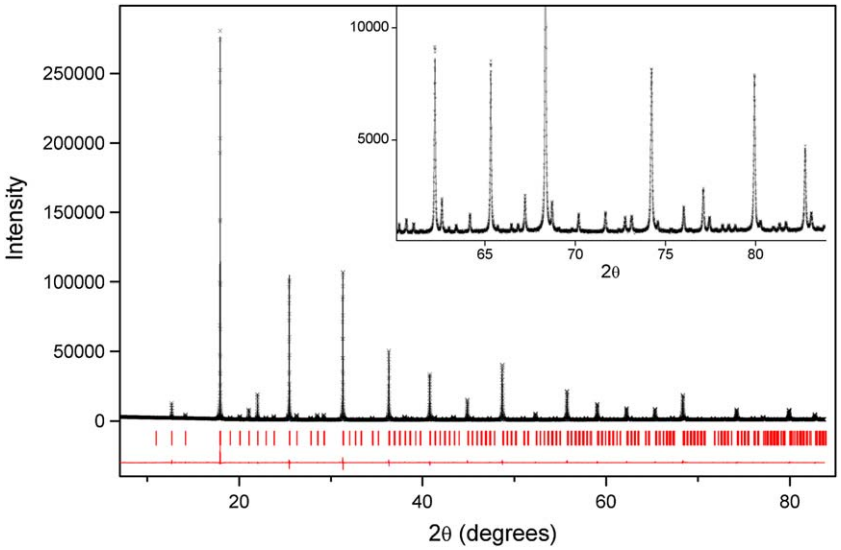

Fig. 2. Observed, calculated and difference X-ray diffraction pattern for $Sr_{0.1}Ca_{0.8}Nd_{0.1}MnO_3$ at room temperature. The insert highlights the quality of both the data and the fit.

Table 1
Structural parameters for the series $Sr_xCa_{0.9-x}Nd_{0.1}MnO_3$ from the Rietveld refinements of synchrotron XRD data collected at room temperature.

x	0.9	0.8	0.7	0.6	0.5	0.4	0.3	0.2	0.1	0.0
Space group	$Pm\bar{3}m$	$Pm\bar{3}m$	*I*4/*mcm*	*I*4/*mcm*	*I*4/*mcm*	*Pbnm*	*Pbnm*	*Pbnm*	*Pbnm*	*Pbnm*
a (Å)	3.8122(1)	3.8065(1)	5.3633(2)	5.3442(2)	5.3284(3)	5.3546(2)	5.3420(1)	5.3257(1)	5.3090(1)	5.2927(2)
b (Å)	= *a*	= *a*	= *a*	= *a*	= *a*	5.3372(3)	5.3286(1)	5.3187(1)	5.3103(1)	5.3051(1)
c (Å)	= *a*	= *a*	7.6398(5)	7.6373(4)	7.6463(7)	7.5495(5)	7.5400(2)	7.5242(1)	7.5058(1)	7.4877(2)
A										
x	1/2	1/2	0	0	0	0.0010(2)	−0.0017(2)	−0.0032(3)	−0.0038(2)	−0.0047(3)
y	1/2	1/2	1/2	1/2	1/2	0.5096(1)	0.5146(1)	0.5196(1)	0.5245(0)	0.5295(1)
z	1/2	1/2	1/4	1/4	1/4	1/4	1/4	1/4	1/4	1/4
O1										
x	–	–	0	0	0	0.0536(7)	0.0618(6)	0.0596(9)	0.0631(7)	0.0675(7)
y	–	–	0	0	0	0.9963(8)	0.9947(5)	0.9918(4)	0.9916(3)	0.9896(4)
z	–	–	1/4	1/4	1/4	1/4	1/4	1/4	1/4	1/4
O2										
x	1/2	1/2	0.2359(7)	0.2280(4)	0.2236(6)	0.2345(8)	0.2732(4)	0.2761(5)	0.2829(4)	0.2864(4)
y	0	0	*x*+1/2	*x*+1/2	*x*+1/2	0.2723(6)	0.2234(4)	0.2181(5)	0.2169(4)	0.2150(4)
z	0	0	0	0	0	−0.0224(4)	−0.0227(3)	−0.0271(4)	−0.0304(3)	−0.0318(3)
R_p (%)	7.32	7.32	10.17	8.38	10.55	4.99	3.96	3.5	3.91	4.05
R_{wp} (%)	10.54	10.54	14.49	12.27	16.01	6.8	5.33	4.86	5.05	6.02
Mn–O1/Å	1.9061(1)	1.9032(1)	1.9100(1)	1.9093(1)	1.9116(1)	1.904(1)	1.914(1)	1.908(1)	1.907(1)	1.907(1)
Mn–O2 (Å)			1.8992(3)	1.8968(3)	1.8943(5)	1.928(4)	1.891(2)	1.884(3)	1.906(3)	1.912(2)
Mn–O2 (Å)						1.878(4)	1.915(2)	1.926(3)	1.908(3)	1.903(2)
O2–Mn–O2	90	90	90	90	90	90.75(3)	90.68(2)	90.87(3)	90.81(3)	90.72(3)
Δd[a]	0	0	3.58	4.80	9.21	57.54	16.90	40.74	0.092	1.86

In all cases the Mn is at (0,0,0).

[a] $\Delta d = (\frac{1}{6}) \sum \left[\frac{d_n - \langle d \rangle}{\langle d \rangle}\right]^2$.

X-point reflections were clearly evident in the diffraction patterns. The tendency for perovskites to display high metric symmetry whilst retaining a strongly distorted structure is well known and is a feature of the $Sr_{1-x}Ce_xMnO_3$ oxides [6,8]. The systematic shift of the (222) reflection to higher angles, evident in Fig. 1, with increased Ca content reflects the decrease in the cell size due to the smaller size of Ca^{2+} cf Sr^{2+} (1.34 vs 1.44 Å) [21].

The structures were then refined from the synchrotron X-ray diffraction profiles. A representative example of a Rietveld plot is given in Fig. 2 and the results are summarised in Table 1.

Perusal of Table 1 illustrates a number of points. Firstly the precision of the structural refinements, as described by the esds, is very high even for the oxygen anions, enabling detailed analysis of both the cell parameters and atomic contacts (bond lengths and angles). In keeping with the symmetry, the esds for the anion positions are larger in the lower symmetry structures. Secondly the *R*-factors for the tetragonal oxides are noticeably higher than those for either the cubic or orthorhombic structures. This is a consequence of anisotropic broadening of certain reflections associated with the CJTD of the MnO_6 octahedra. Although not explicitly discussed by Kato et al. [22] these workers also observed (as reproduced in their Fig. 1) unusual peak shapes in tetragonal $Sr_{0.65}Nd_{0.35}MnO_3$. Thirdly in all cases the individual Mn–O bond lengths are unexceptional, although the refinements suggest a

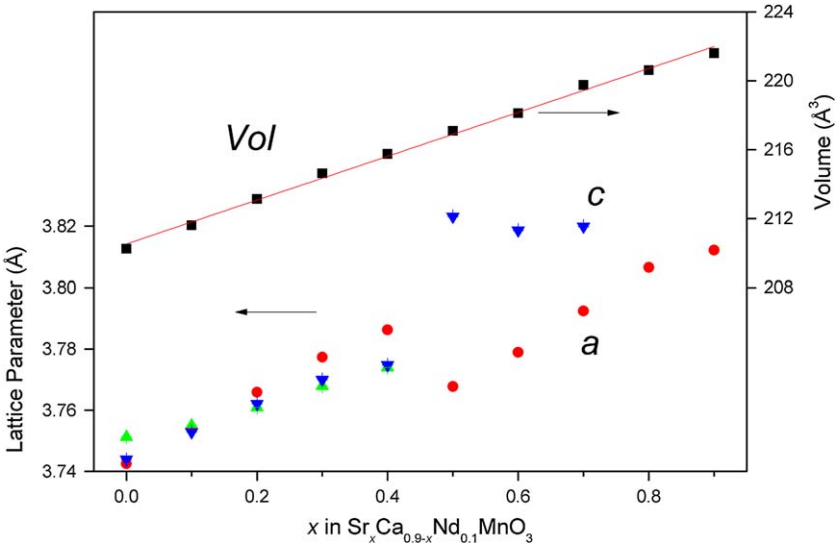

Fig. 3. Variation of the reduced lattice parameters and the appropriate scaled cell volume with composition in $Sr_xCa_{0.9-x}Nd_{0.1}MnO_3$. For $x \leq 0.40$ the structures are in *Pbnm*, and for $x \geq 0.8$ the structures are cubic in $Pm\bar{3}m$. At intermediate composition the structures are in *I*4/*mcm*. Where not apparent the esds are smaller than the symbols.

Table 2
Structural parameters for the series $Sr_xCa_{0.8-x}Nd_{0.2}MnO_3$ from the Rietveld refinements of synchrotron XRD data collected at room temperature.

X	0.8	0.7	0.6	0.5	0.4	0.3	0.3	0.2	0.1	0.0
Space group	*I*4/*mcm*	*I*4/*mcm*	*I*4/*mcm*	*I*4/*mcm*	*I*4/*mcm*	*I*4/*mcm*	*Pbnm*	*Pbnm*	*Pbnm*	*Pbnm*
a (Å)	5.36700(2)	5.34760(2)	5.33260(1)	5.31760(2)	5.30370(2)	5.29330(3)	5.322(2)	5.35020(2)	5.32560(4)	5.31640(4)
b (Å)	= *a*	= *a*	= *a*	= *a*	= *a*	= *a*	5.324(2)	5.34060(3)	5.33080(4)	5.32700(4)
c (Å)	7.74630(3)	7.75560(5)	7.75110(3)	7.75310(4)	7.75180(4)	7.74040(6)	7.655(2)	7.54640(3)	7.54440(5)	7.51400(6)
A										
x	0	0	0	0	0	0		−0.0044(2)	0.0035(3)	−0.0584(3)
y	1/2	1/2	1/2	1/2	1/2	1/2		0.5278(1)	0.5219(1)	0.9933(6)
z	1/4	1/4	1/4	1/4	1/4	1/4		1/4	1/4	1/4
O1										
x	0	0	0	0	0	0		0.0750(11)	−0.0584(6)	0.0614(10)
y	0	0	0	0	0	0		0.9878(6)	0.9933(6)	0.9933(6)
z	1/4	1/4	1/4	1/4	1/4	1/4		1/4	1/4	1/4
O2										
x	0.2345(6)	0.2288(6)	0.2218(4)	0.2183(4)	0.2148(4)	0.2101(5)		0.2858(7)	0.2798(10)	0.2793(11)
y	*x*+1/2	*x*+1/2	*x*+1/2	*x*+1/2	*x*+1/2	*x*+1/2		0.2174(7)	0.2159(10)	0.2156(10)
z	0	0	0	0	0	0		−0.0291(7)	0.0318(10)	−0.0292(11)
R_p (%)	8.72	9.69	9.15	9.02	7.46	7.2		4.91	5.91	4.69
R_{wp} (%)	12.27	14.13	12.64	12.77	10.73	10.83		6.76	8.25	7.39
Mn–O1 (Å)	1.9366(1)	1.9389(1)	1.9378(1)	1.9383(1)	1.9380(1)	1.9351(1)		1.922(1)	1.912(1)	1.915(1)
Mn–O2 (Å)	1.9012(3)	1.8975(4)	1.8974(3)	1.8951(4)	1.8936(4)	1.895(9)		1.923(7)	1.898(3)	1.930(4)
Mn–O2 (Å)								1.900(7)	1.893(3)	1.931(4)
O2–Mn–O2								90.76(4)	90.87(6)	90.55(4)
Δd	228.29	312.79	298.00	341.22	360.86	294.36		92.17	53.68	43.34

In all cases the Mn is at (0,0,0). The sample with $x = 0.3$ contains both the tetragonal and orthorhombic phases but atomic positions could not be refined reliably for the orthorhombic phase.

small but significant elongation of the MnO_6 octahedra exists in the tetragonal structures. This elongation is not apparent in either the orthorhombic or cubic structures and is a hallmark of a cooperative Jahn–Teller distortion (CJTD). The current refinements do not suggest there is a $d_{x^2-r^2}$ type *OO* in the orthorhombic phase, that would be indicated by the presence of two long Mn–O bonds in the *ab* plane as seen from $LaMnO_3$ [10]. That the bond length anisotropy in the tetragonal structures is small is hardly surprising given that only 10% of the Mn is present in the JT active Mn^{3+} state.

The composition dependence of the lattice parameters and cell volumes for the series $Sr_xCa_{0.9-x}Nd_{0.1}MnO_3$ are illustrated in Fig. 3 and demonstrate a progressive increase in the cell volume as the amount of the larger Sr^{2+} (ionic radii 1.44 Å cf 1.34 Å for Ca^{2+}) increases. In contrast to this smooth variation there is an abrupt discontinuity in the lattice parameters near $x = 0.5$, corresponding to the orthorhombic–tetragonal transition. This transition is associated with the removal of the large tetragonal distortion evident in the *I*4/*mcm* phases. In comparison to the almost linear increase of the *a*-parameter in the tetragonal phase as the Sr content increases, the *c*-parameter remains essentially constant. The composition steps are not sufficiently small to establish if the composition induced $I4/mcm-Pm\bar{3}m$ transition occurs abruptly, as in the series $Sr_{1-x}Ce_xMnO_3$ [6,9], or continuously as in the series $Sr_{1-x}Ca_xTiO_3$ [23].

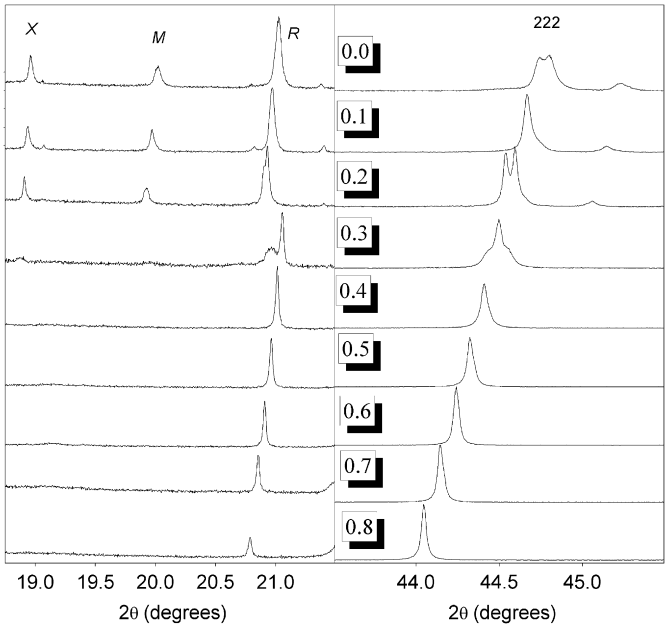

Fig. 4. Selected portions of the observed synchrotron X-ray powder diffraction patterns for members in the series $Sr_xCa_{0.8-x}Nd_{0.2}MnO_3$. The format is the same as in Fig. 1. Note the unusual peak shapes for the $x = 0.3$ sample as a consequence of the co-existence of the *Pbnm* and *I*4/*mcm* phases.

The absence of an intermediate orthorhombic *Imma* phase in this series is noteworthy. This phase is observed in both the $Sr_{1-x}Ce_xMnO_3$ [6,9] and $Sr_{1-x}Pr_xMnO_3$ [13] perovskites but it is neither observed in the series $Sr_{1-x}Ca_xMnO_3$ that also exhibits a composition induced orthorhombic–tetragonal transition [24], nor was it observed in the series $Sr_{1-x}La_xMnO_3$ where a rhombohedral phase exists [15]. Following from the early work of Caignaert et al. [25], Kajimoto et al. [26] demonstrated that the *Imma* phase exists in the $Sr_{1-x}Nd_xMnO_3$ manganites at higher Nd contents. Evidently the Ca cations suppress the formation of the *Imma* phase although the basis for this is unclear. Finally the changes in the lattice parameters in the orthorhombic phase suggest an evolution in the structure from one with $a > b$ to one with $b > a$. This progressive change is responsible for the loss of the apparent splitting of the (222) reflection illustrated in Fig. 1 and is reminiscent of the temperature dependence of the lattice parameters in $CaMnO_3$ [27]. Zhou and Goodenough [28] have suggested that the crossover of *b* and *a* in orthorhombic perovskites is a consequence of competition between the rotation of the octahedra, necessary to accommodate the bonding requirements of the *A*- and *B*-type cations, as quantified by the tolerance factor, and the distortion of the BO_6 octahedron. Distortion of the BO_6 octahedra can occur by the variation of the individual *B*–O bond/lengths and/or of the O–*B*–O bond angles. As evident from Tables 1 and 2 the distortion of the MnO_6 octahedra in the present series varies appreciably across both the series of compounds and it is inappropriate to describe the octahedra as rigid units.

Increasing the Nd content to $y = 0.2$ is expected to both increase the extent of the CJTD and to favour the lower symmetry

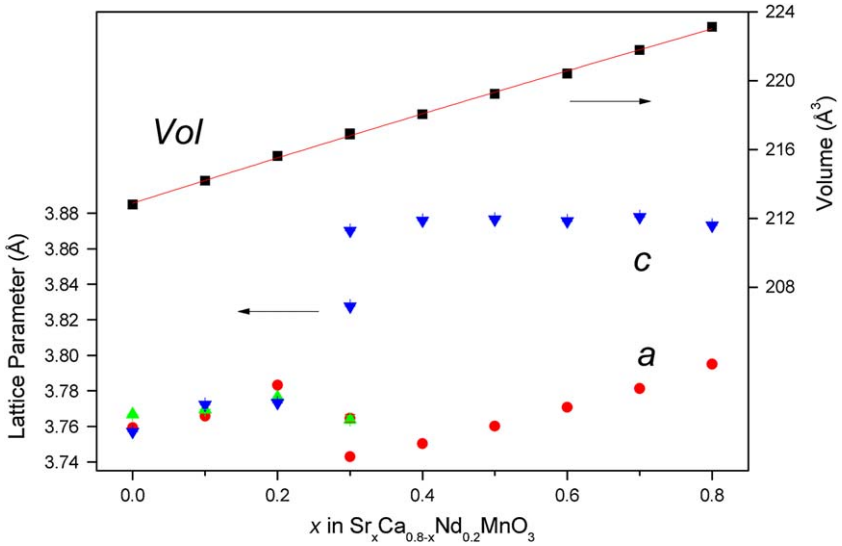

Fig. 5. Variation of the reduced lattice parameters and the appropriate scaled cell volume with composition in $Sr_xCa_{0.8-x}Nd_{0.2}MnO_3$. For $x \leq 0.20$ the structures are orthorhombic in *Pbnm* and for $x \geq 0.4$ the structures are tetragonal in *I*4/*mcm*. The sample with $x = 0.3$ is a mixture of these two phases.

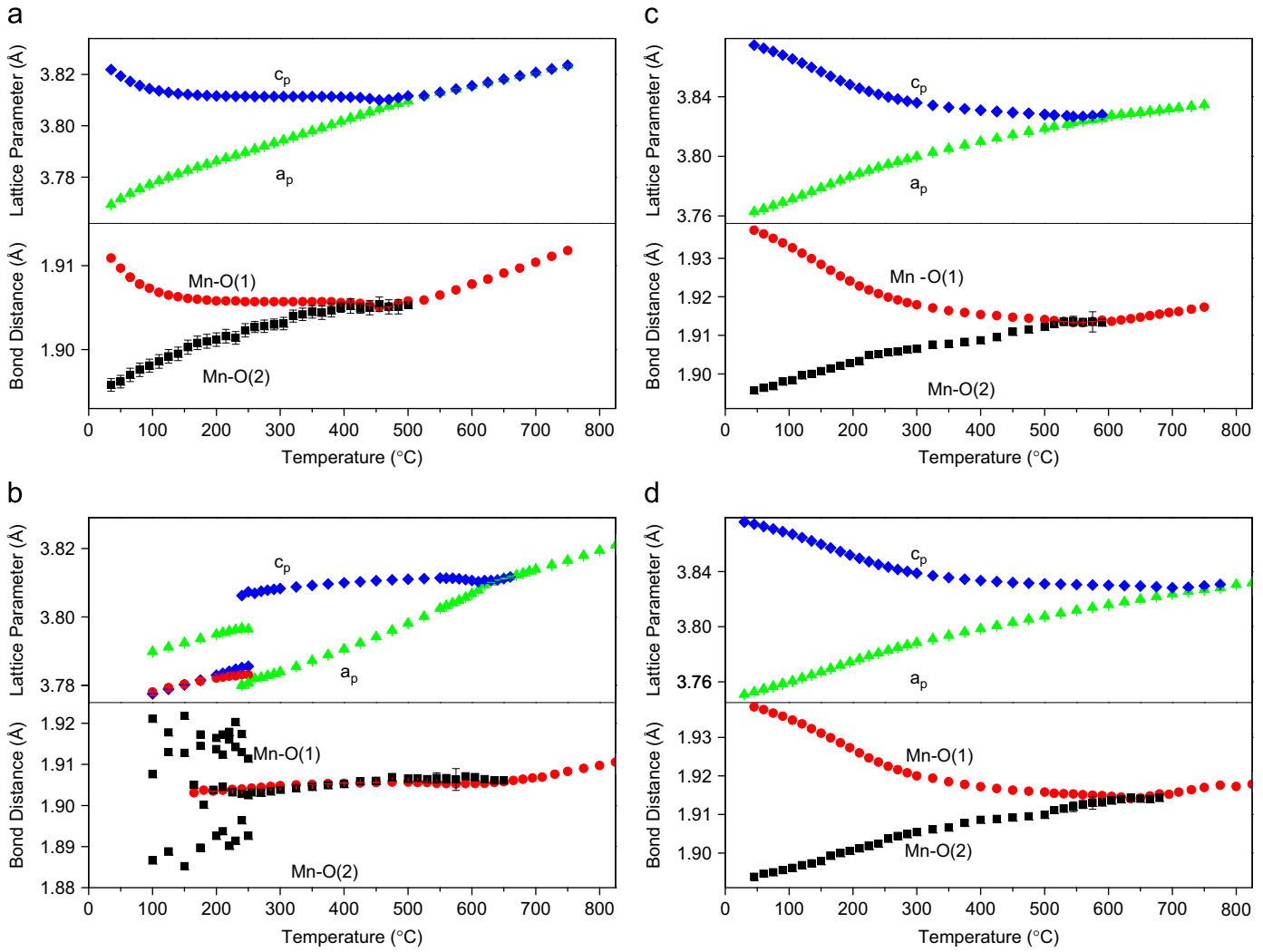

Fig. 6. Temperature dependence of the lattice parameters and Mn–O bond lengths for selected members of the $Sr_xCa_{0.9-x-y}Nd_yMnO_3$ series. The lattice parameters have been reduced to the equivalent values in the primitive perovskite for clarity. For clarity the esds in the bond distances in the orthorhombic phase have not been illustrated, in all others where these are not apparent they are smaller than the symbols. In (a), (c) and (d) the transitions from tetragonal ($I4/mcm$) to cubic ($Pm\bar{3}m$) occur near 510, 600 and 790 °C, respectively. For $Sr_{0.4}Ca_{0.5}Nd_{0.1}MnO_3$ shown in (b) the structure evolves from orthorhombic in $Pnma$ $T<160$ °C, to mixed $Pnma$ and $I4/mcm$ $240<T<260$ °C to pure tetragonal in $I4/mcm$ $260<T<660$ °C, and finally pure cubic in $Pm\bar{3}m$ above 670 °C. (a) $Sr_{0.5}Ca_{0.4}Nd_{0.1}MnO_3$, (b) $Sr_{0.4}Ca_{0.5}Nd_{0.1}MnO_3$, (c) $Sr_{0.5}Ca_{0.3}Nd_{0.2}MnO_3$ and (d) $Sr_{0.4}Ca_{0.4}Nd_{0.2}MnO_3$.

structures since Nd^{3+} is smaller than Sr^{2+} (1.27 vs 1.44 Å) [21]. This expectation is realised as shown in Fig. 4 where $Sr_{0.8}Nd_{0.2}MnO_3$ is observed to be tetragonal and the transition to orthorhombic, as evident from both the splitting of the cubic (222) reflection and the growth of the diagnostic M- and X-point reflections occurs near $x=0.3$, that is at $Sr_{0.3}Ca_{0.5}Nd_{0.2}MnO_3$. That we find $Sr_{0.8}Nd_{0.2}MnO_3$ is tetragonal is in contrast to the results of Nagao et al. [29] who reported their sample of this composition to be a mixture of $I4/mcm+Pm\bar{3}m$. We postulate that this difference reflects the very different synthetic conditions utilised by Nagao et al. [29], who prepared single crystals using a floating zone furnace.

It is evident from Fig. 4 that the diffraction pattern of $Sr_{0.3}Ca_{0.5}Nd_{0.2}MnO_3$ is unusual. Rietveld analysis demonstrated that this exists as a mixture of $Pbnm$ and $I4/mcm$. The results for the Rietveld analysis of this series are collected in Table 2. As noted for the $y=0.1$ series the MnO_6 octahedra in the tetragonal oxides show a significant tetragonal elongation, and not surprisingly this is larger than in the $y=0.2$ series.

Fig. 5 confirms the deductions made from the $y=0.1$ series, especially that the c-parameter in the tetragonal phase is essentially independent of composition, whereas the a-parameter shows an approximately linear increase as the Sr content increases. The cell volume shows a continuous evolution across the full series; however, the individual cell parameters rapidly change at a critical composition, $x=0.3$, where the $Pbnm$ and $I4/mcm$ phases co-exist. The volume of the orthorhombic and tetragonal phases in the $x=0.3$ sample are, within the precision of the present study, identical. Finally we again observe the evolution in the orthorhombic structure from one with $a>b$ to one with $b>a$, although as was found for the $y=1$ series the distortion of the cell metric in the orthorhombic phase is much less than in the tetragonal phase.

The temperature dependent behaviour of the structures for four selected samples, with $y=0.1$, $x=0.4$ or 0.5 and $y=0.2$, $x=0.4$ or 0.5, was investigated using high temperature synchrotron X-ray diffraction. Heating the tetragonal oxide $Sr_{0.5}Ca_{0.4}Nd_{0.1}MnO_3$ above 500 °C results in an apparently continuous transition from the tetragonal, $I4/mcm$, structure to one in cubic, $Pm\bar{3}m$. The precision in determining the atomic coordinates of the oxygen anion at the 8h site $(x, x+\frac{1}{2}, 0)$ afforded by our synchrotron X-ray measurements yields, accurate Mn–O bond

distances and the tilt angle between the MnO_6 octahedra, given by $\tan\varphi = 4u$ where $u = x - \frac{1}{4}$. The temperature dependence of these features is displayed in Figs. 6 and 7, respectively.

The tetragonal $I4/mcm$ structure ($a^0a^0c^-$ tilt system) is characterised by out-of-phase tilting of the MnO_6 octahedra around the tetragonal axis. This tilting is, obviously, absent in the cubic structures. The magnitude of this tilting can serve as an order parameter for the tetragonal-to-cubic phase transition [30]. As evident from Fig. 7, for the four compositions investigated the tilt angle varies continuously throughout this temperature range and in each case it is well fitted to an expression of the form $\varphi \propto (T_c - T)^{1/3}$, where T_c is the cubic transition temperature suggestive of a tricritical phase transition.

The temperature dependence of the amplitude of the R_4^+ mode responsible for the breaking of symmetry to the tetragonal $I4/mcm$ space group was investigated using the program AMPLIMODES [31]. AMPLIMODES uses experimentally determined structures of the high and low symmetry phases to perform a symmetry-mode analysis of a displacive phase transition. The amplitude of the R_4^+ mode showed similar temperature dependence on the tilt angle for the four investigated compositions demonstrating that the tilting of the octahedra is the primary order parameter associated with the tetragonal to cubic phase transitions. Faik et al. [32] have recently reported a similar correlation in tetragonal–cubic transition of the cation ordered perovskite, Sr_2CrSbO_6.

Both the lattice parameters of and the bond distances in $Sr_{0.5}Ca_{0.4}Nd_{0.1}MnO_3$ show a rapid initial decrease in the tetragonal distortion upon heating to around 100 °C, before undergoing a more gradual change, with the structure eventually becoming cubic above 500 °C. This change in behaviour is more evident in the tetragonal strain, estimated as $\varepsilon_t = c_p - a_p/c_p + a_p$, where the temperature dependence of the tetragonal strain shows two linear regions (see Fig. 8).

Increasing the Ca content in the series $Sr_xCa_{0.9-x}Nd_{0.1}MnO_3$ to $x = 0.4$, that is to $Sr_{0.4}Ca_{0.5}Nd_{0.1}MnO_3$, results in a transition to the orthorhombic $Pbnm$ structure at room temperature. The temperature dependence of the lattice parameters of, and Mn–O bond distances in, this oxide, illustrated in Fig. 6, show a distinct first order $Pbnm$–$I4/mcm$ transition near 250 °C and a second continuous $I4/mcm$–$Pm\bar{3}m$ transition near 660 °C. The former transition is characterised by the co-existence of the two phases between

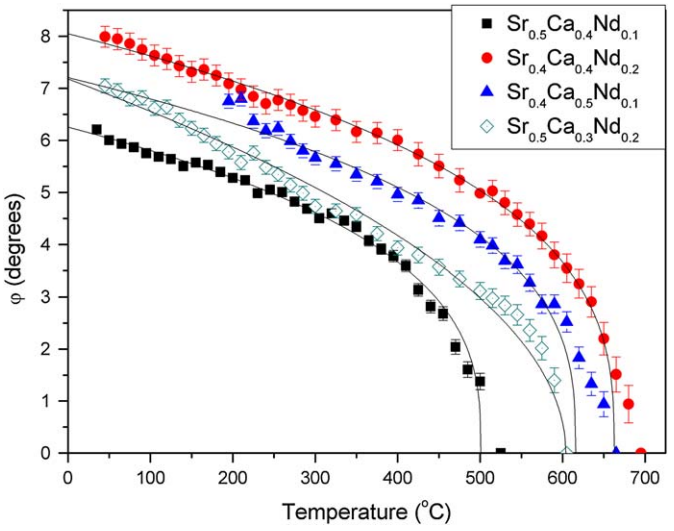

Fig. 7. Temperature dependence of the tilt angle for selected members of the $Sr_xCa_{0.9-x-y}Nd_yMnO_3$ series. The solid lines are calculated using a $(T_c - T)^{1/3}$ relationship.

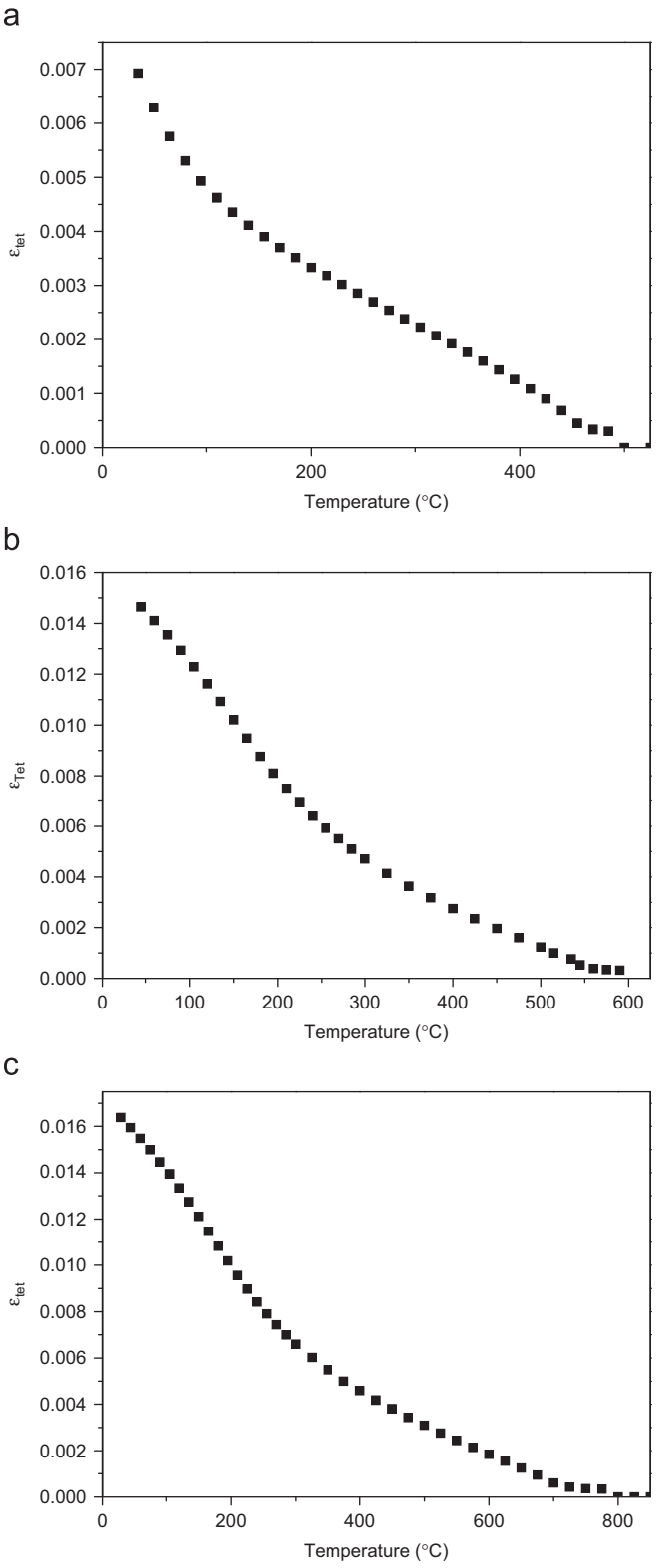

Fig. 8. Temperature dependence of the tetragonal strains. (a) $Sr_{0.5}Ca_{0.4}Nd_{0.1}MnO_3$, (b) $Sr_{0.5}Ca_{0.3}Nd_{0.2}MnO_3$ and (c) $Sr_{0.4}Ca_{0.4}Nd_{0.2}MnO_3$.

240 and 260 °C, whilst it is possible to obtain accurate lattice parameters in this region the refined atomic coordinates have large esds, limiting the analysis of these results. Nevertheless it is apparent from Fig. 6 that the tetragonal distortion of the $I4/mcm$ phase progressively reduces upon heating. Importantly the two crystallographically unique Mn–O bond distances in the

tetragonal phase are essentially equal demonstrating the absence of a CJTD. The temperature dependence of the tetragonal strain does not show any evidence of the two processes in this oxide. Evidently the 10% Mn^{3+} that forms by partially replacing Sr^{2+} with Nd^{3+} is insufficient to stabilise a JT distorted structure in the tetragonal phase of $Sr_{0.4}Ca_{0.5}Nd_{0.1}MnO_3$, once this forms above 250 °C, just as it was insufficient to do so in $Sr_{0.5}Ca_{0.4}Nd_{0.1}MnO_3$ above 150 °C.

$Sr_{0.5}Ca_{0.3}Nd_{0.2}MnO_3$ transforms to the cubic structure at a similar temperature, ~600 °C, to that observed for $Sr_{0.4}Ca_{0.5}Nd_{0.1}MnO_3$, reflecting their similar tolerance factors $t = 1.005$ and 1.010, respectively. The structure of $Sr_{0.5}Ca_{0.3}Nd_{0.2}MnO_3$ is, however, tetragonal at room temperature. The thermal evolution of both the lattice parameters and the bond distances for this oxide clearly show two regions, one of rapid change below ~250 °C, followed by a more gradual reduction in the tetragonal distortion. This change in the nature of the transition is clearly evident in the tetragonal strain. The experimentally observed behaviour of the tetragonal structure in $Sr_{0.5}Ca_{0.3}Nd_{0.2}MnO_3$ is remarkably similar to that of $Sr_{0.4}Ca_{0.4}Nd_{0.2}MnO_3$, the most significant difference being the increase in the ultimate transition temperature as evident for the variation in the tilt angles. A significant feature of these results is that the inflection point in the tetragonal strain occurs at approximately the same temperature (~250 °C) in these two samples, and this is clearly higher than in $Sr_{0.5}Ca_{0.4}Nd_{0.1}MnO_3$ where it is closer to 100 °C. This suggests that, despite the transition to the cubic structure requiring much higher temperatures in $Sr_{0.4}Ca_{0.4}Nd_{0.2}MnO_3$ compared to $Sr_{0.5}Ca_{0.3}Nd_{0.2}MnO_3$ the thermal energy necessary to drive the first transition is approximately equal in these two samples and it is much higher than in $Sr_{0.5}Ca_{0.4}Nd_{0.1}MnO_3$. The temperature of the inflection point in the former two samples is in reasonable agreement with the *OO* temperature reported for $Sr_{0.8}Nd_{0.2}MnO_3$ by Kuwahara and co-workers [33]. Analysis of our previously published data [24] for the closely related oxide $Ca_{0.5}Sr_{0.5}MnO_3$ that does not contain any Mn^{3+} ions demonstrates the tetragonal strain to vary lineally with temperature.

There is now a substantial body of evidence that JT manganites can undergo isosymmetric phase transitions associated with the removal of a JT distortion. In some oxides, such as $LaMnO_3$, this transition is strongly first order [34]; however, in some manganites, including the present series of $Sr_xCa_{1-x-y}Nd_yMnO_3$ oxides the transition appears continuous. Recent studies of $LaMnO_3$ have suggested that short range *OO* nanoclusters persist above the *OO* transition temperature [35,36], an observation that is consistent with a first order transition. A feature of the structural phase transitions is that the magnitude of the cooperative tilting of the MnO_6 octahedra is apparently unaffected by the removal of the JT distortion. The significance of this observation must be treated with some caution since the magnitude of the tilt angle can remain unaltered through a first order transition as exemplified by $PrAlO_3$ where the first order $R\bar{3}c$ to *Imma* transition involves a reorientation of the tilt axis from (111) to (110) [30].

The above results, together with our previous studies of $Sr_xCe_{1-x}MnO_3$ and doped variants thereof [6–8], and of $SrRu_{0.5}Mn_{0.5}O_3$ [11] demonstrate the presence of an isosymmetric $I4/mcm$ to $I4/mcm$ phase transition associated with the removal of long range orbital ordering or the CJTD. Such a transition has been observed previously in $LaMnO_3$ where a strongly first order $O' \rightarrow O$ (*Pbnm–Pbnm*) transition is observed where O' describes the *OO* structure [34]. By analogy with this we label the low temperature $I4/mcm$ structure that features both CJTD of the MnO_6 octahedra and cooperative tilting of these as T' and the high temperature structure that features only a tilting distortion as T. The $T' \rightarrow T$ transition involves the loss of the CJTD. A feature of the $I4/mcm$ structure is that the tilting distortion responsible for the lowering of the symmetry from $Pm\bar{3}m$ to $I4/mcm$ also lowers the local symmetry of the *B*-site cation from O_h to D_{4h} allowing for a tetragonal elongation (or compression) of the BO_6 octahedra. Such a distortion must remove the degeneracy of the e_g orbitals in a transition metal cation as is required by the JT theorem. In this regard the tilting transition is analogous to the Q_3 type distortion of a JT cation [4].

The above does not demand that the two distortions co-exist and it is easy to imagine structures that exhibit *OO* but not octahedral tilting as evidenced by $KCuF_3$ [37]. Nevertheless the coexistence of the two distortions in tetragonal manganites might therefore be anticipated. Carpenter and Howard have recently confirmed, using group theory, that irrespective of which distortion (JT or tilting) occurs first the application of both R_4^+ and Γ_3^+ mode yields the same tetragonal structure [38]. It is unlikely that both distortions will have identical stabilities, leading to the sequential loss of these. An apparent exception to this comes from diffraction and TEM studies of single crystals of $Sr_{0.8}Nd_{0.2}MnO_3$ by Nagao et al. [29] revealing the existence of a two-phase $I4/mcm + Pm\bar{3}m$ mixture demonstrating the existence of a first order transition between these. We speculate that this is a consequence of the simultaneous loss of *OO* and cooperative tilting. The coexistence of these phases is analogous to that seen in $LaMnO_3$ [35,36].

In conclusion, synchrotron X-ray powder diffraction studies of the perovskite manganites $Sr_xCa_{1-x-y}Nd_yMnO_3$ with $y = 0.1$ or 0.2 show the structure of these to change from $Pm\bar{3}m \leftrightarrow I4/mcm \leftrightarrow Pbnm$ depending on the cation distribution. Orbital ordering is apparent in the tetragonal oxides, as revealed by the large tetragonal elongation of the MnO_6 octahedra. Heating selected examples demonstrate the presence of, an apparently continuous, isosymmetric $I4/mcm$ to $I4/mcm$ phase transition associated with the removal of long range orbital ordering. A feature of such transitions is the continuous evolution of the octahedral tilt angle through the $I4/mcm$ to $I4/mcm$ phase transition. Heating to still higher temperatures results in a continuous transition to the cubic $Pm\bar{3}m$ structure.

Acknowledgments

This work was, in part, performed at the powder diffraction beamline at the Australian Synchrotron. B.J.K. acknowledges the support of the Australian Research Council for this work.

References

[1] H.A. Jahn, E. Teller, Proceedings of the Royal Society of London Series A—Mathematical and Physical Sciences 161 (1937) 220.
[2] E. Dagotto, Reviews of Modern Physics 66 (1994) 763.
[3] E. Dagotto, T. Hotta, A. Moreo, Physics Reports—Review Section of Physics Letters 344 (2001) 1.
[4] J.B. Goodenough, Annual Review of Materials Science 28 (1998) 1.
[5] R. Maezono, S. Ishihara, N. Nagaosa, Physical Review B 58 (1998) 11583.
[6] B.J. Kennedy, P.J. Saines, Q. Zhou, Z. Zhang, M. Matsuda, M. Miyake, Journal of Solid State Chemistry 181 (2008) 2639.
[7] Z.M. Zhang, C.J. Howard, B.J. Kennedy, M. Matsuda, M. Miyake, Journal of Physics—Condensed Matter 21 (2009) 8.
[8] B.J. Kennedy, J. Ting, Q. Zhou, Z. Zhang, M. Matsuda, M. Miyake, Journal of Solid State Chemistry 182 (2009) 954.
[9] A. Sundaresan, J.L. Tholence, A. Maignan, C. Martin, M. Hervieu, B. Raveau, E. Suard, European Physical Journal B 14 (2000) 431.
[10] J. Rodriguez-Carvajal, M. Hennion, F. Moussa, A.H. Moudden, Physical Review B 57 (1998) R3189.
[11] B.J. Kennedy, Q.D. Zhou, Solid State Communications 147 (2008) 208.
[12] M. Cheah, P.J. Saines, B.J. Kennedy, Journal of Solid State Chemistry 179 (2006) 1775.
[13] K. Knizek, J. Hejtmanek, Z. Jirak, C. Martin, M. Hervieu, B. Raveau, G. Andre, F. Bouree, Chemistry of Materials 16 (2004) 1104.
[14] S. Kolesnik, B. Dabrowski, O. Chmaissem, Z. Bukowski, J. Mais, Journal of Applied Physics 89 (2001) 7407.

[15] O. Chmaissem, B. Dabrowski, S. Kolesnik, J. Mais, J.D. Jorgensen, S. Short, Physical Review B 67 (2003) 094431.
[16] A.G. Christy, Acta Crystallographica Section B—Structural Science 51 (1995) 753.
[17] K.S. Wallwork, B.J. Kennedy, D. Wang, in: AIP Conference Proceedings, vol. 879, 2007, p. 879.
[18] B. Hunter, C. Howard, A Computer Program for Rietveld Analysis of X-ray and Neutron Powder Diffraction Patterns, Lucas Heights Research Laboratories, Sydney, 1998, p. 1.
[19] C.J. Howard, H.T. Stokes, Acta Crystallographica Section B—Structural Science 54 (1998) 782.
[20] A.M. Glazer, Acta Crystallographica Section B—Structural Science 28 (1972) 3384.
[21] R.D. Shannon, Acta Crystallographica Section A 32 (1976) 751.
[22] K. Kato, M. Takata, E. Nishibori, M. Sakata, N. Hamada, Y. Moritomo, Journal of the Physical Society of Japan 74 (2005) 2137.
[23] C.J. Ball, B.D. Begg, D.J. Cookson, G.J. Thorogood, E.R. Vance, Journal of Solid State Chemistry 139 (1998) 238.
[24] Q.D. Zhou, B.J. Kennedy, Journal of Solid State Chemistry 179 (2006) 3568.
[25] V. Caignaert, F. Millange, M. Hervieu, E. Suard, B. Raveau, Solid State Communications 99 (1996) 173.
[26] R. Kajimoto, H. Yoshizawa, H. Kawano, H. Kuwahara, Y. Tokura, K. Ohoyama, M. Ohashi, Physical Review B 60 (1999) 9506.
[27] Q.D. Zhou, B.J. Kennedy, Journal of Physics and Chemistry of Solids 67 (2006) 1595.
[28] J.S. Zhou, J.B. Goodenough, Physical Review Letters 94 (2005) 065501.
[29] M. Nagao, T. Asaka, T. Nagai, D. Akahoshi, R. Hatakeyama, T. Yokosawa, M. Tanaka, H. Yoshikawa, A. Yamazaki, K. Kimoto, H. Kuwahara, Y. Matsui, Journal of the Physical Society of Japan 76 (2007) 103706.
[30] M.A. Carpenter, C.J. Howard, B.J. Kennedy, K.S. Knight, Physical Review B 72 (2005) 15.
[31] M.I. Aroyo, J.M. Perez-Mato, C. Capillas, E. Kroumova, S. Ivantchev, G. Madariaga, A. Kirov, H. Wondratschek, Zeitschrift fur Kristallographie. 221 (2006) 15.
[32] A. Faik, J.M. Igartua, M. Gateshki, G.J. Cuello, Journal of Solid State Chemistry 182 (2009) 1717.
[33] D. Akahoshi, R. Hatakeyama, M. Nagao, T. Asaka, Y. Matsui, H. Kuwahara, Physical Review B 77 (2008) 054404.
[34] T. Chatterji, F. Fauth, B. Ouladdiaf, P. Mandal, B. Ghosh, Physical Review B 68 (2003) 052406.
[35] X.Y. Qiu, T. Proffen, J.F. Mitchell, S.J.L. Billinge, Physical Review Letters 94 (2005) 177203.
[36] M.C. Sanchez, G. Subias, J. Garcia, J. Blasco, Physical Review Letters 90 (2003) 214426.
[37] A. Okazaki, Journal of the Physical Society of Japan 26 (1969) 870.
[38] M.A. Carpenter, C.J. Howard, Acta Crystallographica Section B—Structural Science 65 (2009) 134.